

The Impact of Severe Plastic Deformation on the Microstructure and Physicomechanical Properties of Al–0.4Zr

A. M. Mavlyutov^a, T. A. Latynina^{a, b}, M. Yu. Murashkin^{c, d}, R. Z. Valiev^{c, d}, and T. S. Orlova^{a, b, *}

^aSt. Petersburg National Research University of Information Technologies, Mechanics, and Optics, St. Petersburg, Russia

^bIoffe Physical-Technical Institute, Russian Academy of Sciences, St. Petersburg, Russia

^cSt. Petersburg State University, St. Petersburg, Russia

^dUfa State Aviation Technical University, Ufa, Russia

*e-mail orlova.t@mail.ioffe.ru

Received September 19, 2017

Abstract—The influence of high pressure torsion on the microstructure and mechanical and electrical properties is elucidated for an Al–0.4Zr alloy pre-annealed at 648 K for 60 h. The transmission electron microscopy has revealed that the annealing causes the dispersive release of nanoparticles of a secondary Al₃Zr phase. The formation of this structure in the alloy ensures an increase in its conductivity from 50.7 to 58.8% IACS owing to a decrease in the Zr concentration in a solid solution. As established, high pressure torsion processing at room temperature of the pre-annealed alloy leads to the formation of a uniform ultrafine structure in them, as well as to the partial dissolution of Al₃Zr nanoparticles, resulting in higher strength and lower conductivity. It is shown that additional annealing of the ultrafine grained alloy for 1 h at 503 K results in a strength increase by 20% and the recovery of conductivity to the annealed state level (58.3% IACS).

Keywords: aluminum-zirconium alloy, severe plastic deformation, electrical resistivity, microhardness, yield stress, ultimate tensile strength, ultrafine grained structure, nanoscale particles

DOI: 10.1134/S2075113319010210

INTRODUCTION

Aluminum alloys are the promising materials for electrotechnical applications owing to their high conductivity, low density, excellent corrosion resistance, and manufacturability. At present, aluminum alloys used as conductors are required to exhibit high strength and conductivity. It is known that pure Al, when exposed to prolonged operation at temperatures above 363 K, undergoes recrystallization and, consequently, strength degradation [1]. In order to increase the operating temperature, it was proposed to dope the aluminum alloys with transition metals, such as Zr and Sc, or rare-earth (RE) metals [2–7]. Meanwhile, possessing sufficiently high thermal stability of physicomechanical properties during prolonged high-temperature operation, these conducting alloys are characterized by low strength. On the other hand, it was shown in [8] that good thermal stability of the structure and, accordingly, of the strength characteristics is achievable in the Al–8.5RE alloy, where RE = 5.4 wt % Ce and 3.1% wt La. Nevertheless, the use of REs makes the cable products much more expensive. In this respect, the cheaper way to attain the higher thermal stability of aluminum alloys is their doping with such a transition metal as Zr [1, 9]. So, as shown in [3], the doping with Zr in an amount up to 0.3 wt % makes it

possible to achieve the microstructure with thermal resistance better than the embedding of 7 wt % RE. The thermal resistance of strength properties of Zr-doped aluminum alloys is due to the presence of nanoparticles of a secondary Al₃Zr phase emerging as a result of prolonged annealing (60–100 h) in a temperature range of 623–723 K [10].

Severe plastic deformation (SPD) is a reliable route to substantially improve the strength characteristics of Al-based alloys on account of the formation of an ultrafine-grained (UFG) structure in them [11]. Recent studies have revealed that the use of SPD methods can ensure a pronounced increase in strength and electrical conductivity [12], but also makes it possible to attain high values of thermal resistance [8, 13] in conducting aluminum alloys by means of forming a UFG structure and set phase composition. For example, it was demonstrated in [12] that the equal channel angular pressing, followed by the cold drawing of the Al–0.4Mg–0.2Zr alloy, led to the formation of the UFG structure with Al₃Zr nanoparticles providing a good combination of strength, electrical conductivity, and thermal resistance. Furthermore, as shown in study [14], the annealing of a rapidly crystallized Al–Cr–Zr alloy causes the emergence of chromium and zirconium aluminides, and the successive treatment

Table 1. Chemical composition of Al–0.4Zr alloy. The element content is given in wt %

Al	Zr	Si	Fe	V	Zn	Bal.
99.25	0.393	0.023	0.242	0.026	0.018	~0.05

via high pressure torsion (HPT) together with the UFG structure formation initiates their dissolution. The authors of [15] demonstrated the ability of deformation dissolution of 1.5 wt % Zr atoms upon HPT processing and the formation of the abnormally oversaturated solid solution.

The present work is aimed at the investigation of the influence of HPT and successive annealings on the microstructure and physicochemical properties of the Al–0.4 wt % Zr alloy.

SAMPLES AND EXPERIMENTAL PROCEDURES

Samples were Al–0.4Zr alloys, whose chemical composition is given in Table 1. The cylindrical workpieces with a diameter of 9.5 mm and a height of 8 mm were cut off from the initial rod obtained by the combined casting and rolling. Workpieces were then annealed at 648 K for 60 h. According to data reported in work [16], this thermal treatment makes it possible to form nanoparticles of the Al_3Zr phase (metastable L1_2 modification) in Zr-containing alloys and, consequently, to decrease the Zr atom content in the aluminum matrix. Thus the annealing leads to a substantial decrease in electrical resistivity, whereas the presence of Al_3Zr nanoparticles favors the improvement of the strength of the annealed alloy with respect to the Orowan mechanism [17].

After the pre-annealing, workpieces were subjected to the room-temperature (RT) HPT under a pressure of 6 GPa to ten rotations [11, 18]. This resulted in disk-shaped samples with a diameter of 20 mm and thickness of 1.5 mm; the degree of true deformation in the area at a distance of 5 mm from the center of the disk was $e \approx 6.6$ [18]. A part of samples were then annealed for 1 h at temperatures of 363, 423, 473, 503, and 673 K.

The microstructure of Al–0.4Zr alloys was studied via transmission electron microscopy (TEM) on a JEOL JEM 2100 microscope at an accelerating voltage of 200 kV and by scanning electron microscopy (SEM) using a JSM-6490LV microscope equipped with an

INCA X-sight energy-dispersion analysis consol. Samples were prepared by the spray polishing on a Tenupol-5 setup in a solution of nitric acid (20%) and methanol (80%) at -25°C and a voltage of 15 V. The average size of structural elements was evaluated from a set of at least 200 average diameters measured by means of the ImageJ software program.

The microhardness of samples (H_V) was determined using the Vickers method in accordance with the GOST 2999-75. The exposure time under the load of 1 N was 15 s. Each sample was subjected to at least 15 measurements. The indentation was conducted along the line at a distance of 5 mm from the center of the disk.

In order to perform the mechanical tests tensile samples with a working part width of 2 mm and a length of 6 mm were cut off from on the HPT-processed discs on an electroerosive machine. The schematic of the cutting off and the sample configuration are available in [19]. The uniaxial tensile tests of samples were made on a Shimadzu AG-XD Plus setup with a constant deformation rate of $5 \times 10^{-4} \text{ s}^{-1}$. The deformation of samples was recorded by a TRViewX 55S video extensometer. At least three samples were exposed to tests for each state. The stress–strain diagrams enabled one to determine the yield stress ($\sigma_{0.2}$) corresponding to 0.2% strain, ultimate tensile strength (σ_{UTS}), and relative elongation to failure (δ).

The electrical resistivity was measured via the four-point method at RT and at 77 K in stationary liquid nitrogen (the electrical resistivity at 77 K is labeled hereinafter as ρ_{77}), as well as at several intermediate temperatures of 150–250 K. The temperature of a sample was controlled with a silicon diode at a precision of ± 0.03 K. The resistivity measurement error was $< 2\%$. The resistivity values were used to perform the linear approximation to determine the resistivity at 293 K (ρ_{293}). More details about the specific resistance measurements can be found in our works [20, 21].

RESULTS AND DISCUSSION

Microstructure Evolution

The microstructure of Al–0.4Zr samples was examined via scanning and transmission electron microscopy and by performing a statistical analysis in order to evaluate the average grain size, secondary phase inclusions, and distance between them. Figure 1 displays the initial microstructure of the Al–0.4Zr alloy. It is evident that it consists of subgrains extended in the rolling direction, whose transverse size is about $2 \mu\text{m}$ (see Figs. 1a and 1b). The material structure also exhibits particles of excess crystallization phases that are arranged in lines, being oriented in the rolling direction as are subgrains (see Fig. 1a). The energy-dispersion analysis reveals that these particles are predominantly composed of aluminum and iron. A lack of complementary reflexes in the microdiffraction pattern from the aluminum matrix (see Fig. 1b) indicates the absence of Al_3Zr nanoparticles in the initial structure of the alloy.

Figure 2 shows the bright-field and dark-field images of the microstructure of the Al–0.4Zr alloys after annealing at 648 K for 60 h. As seen the material exposed to the treatment comprises nanoparticles uni-

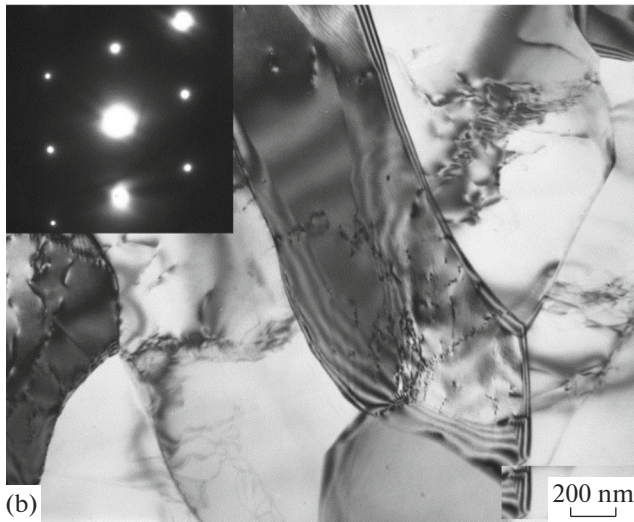
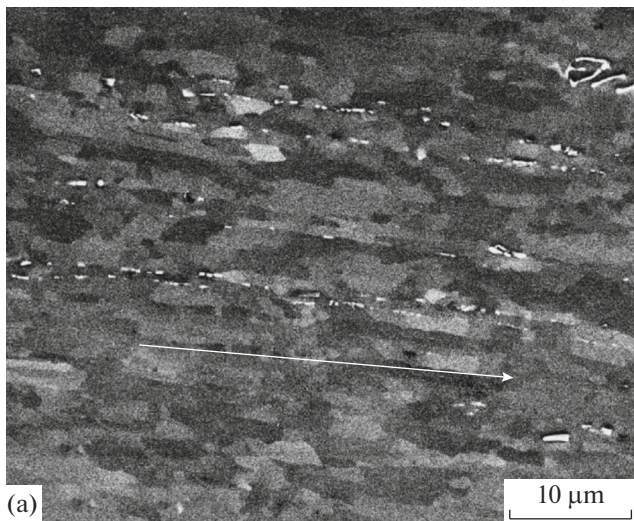


Fig. 1. Initial microstructure of Al–0.4 wt % Zr: (a) back-scattered electron image (SEM), the arrow indicates the rolling direction; (b) bright-field image and microdiffraction pattern ([110] zone axis) (TEM).

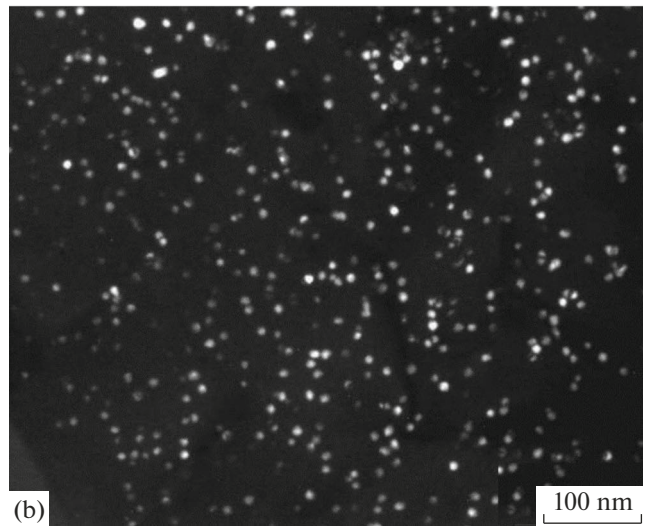
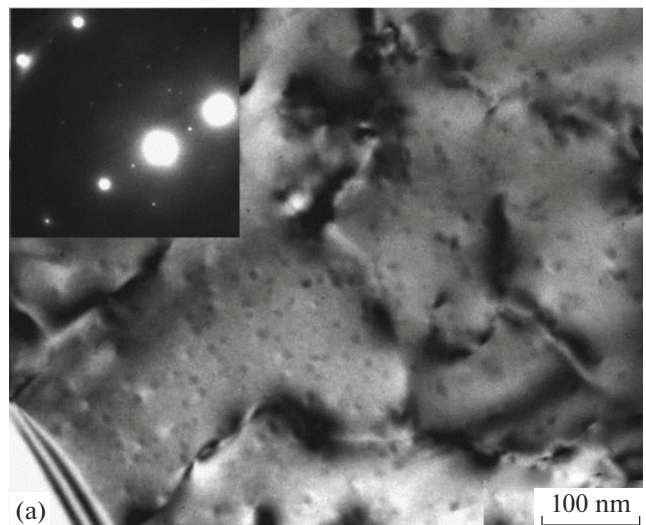


Fig. 2. Microstructure of Al–0.4 wt % Zr annealed at 648 K for 60 h: (a) bright-field image and microdiffraction pattern ([120] zone axis); (b) dark-field image (TEM).

formly distributed within the aluminum matrix. The microdiffraction pattern (see Fig. 2a) with the additional structural reflexes enables these particles to be identified as the secondary Al_3Zr phase of the metastable L_1_2 modification [16]. Figure 2b illustrates the dark-field image of the microstructure in the reflex of the secondary phase. The secondary phase particle size distribution is plotted in Fig. 3a, exhibiting small differences between the values. The average particle size is ~ 13 nm and the average distance between them is ~ 38 nm (Table 2).

HPT causes the formation of the UFG structure in the alloys with the average grain size of ~ 660 nm (Fig. 4a, Table 2) and the pronounced decrease in the nanoparticle concentration. The microdiffraction pattern (see

Fig. 4b) includes no reflexes attributed to the Al_3Zr phase. Meanwhile, the micrographs (Fig. 4) exhibit particles whose average size is ~ 56 nm and the average distance between them is ~ 425 nm (see Table 2). The size distribution diagrams of these ultrafine grains and these particles are plotted in Figs. 3b and 3c, respectively. As follows from the quantitative evaluation, the HPT of alloys leads to their coarsening, but also to a decrease in their volume fraction by an order of magnitude (see Table 2).

Hence, in accordance with microstructural peculiarities detected in alloys exposed to HPT, as well as on the basis of data gathered in [14, 15], it can be assumed that a great amount of nanoscaled Al_3Zr phase has been dissolved. It is worth noting that the

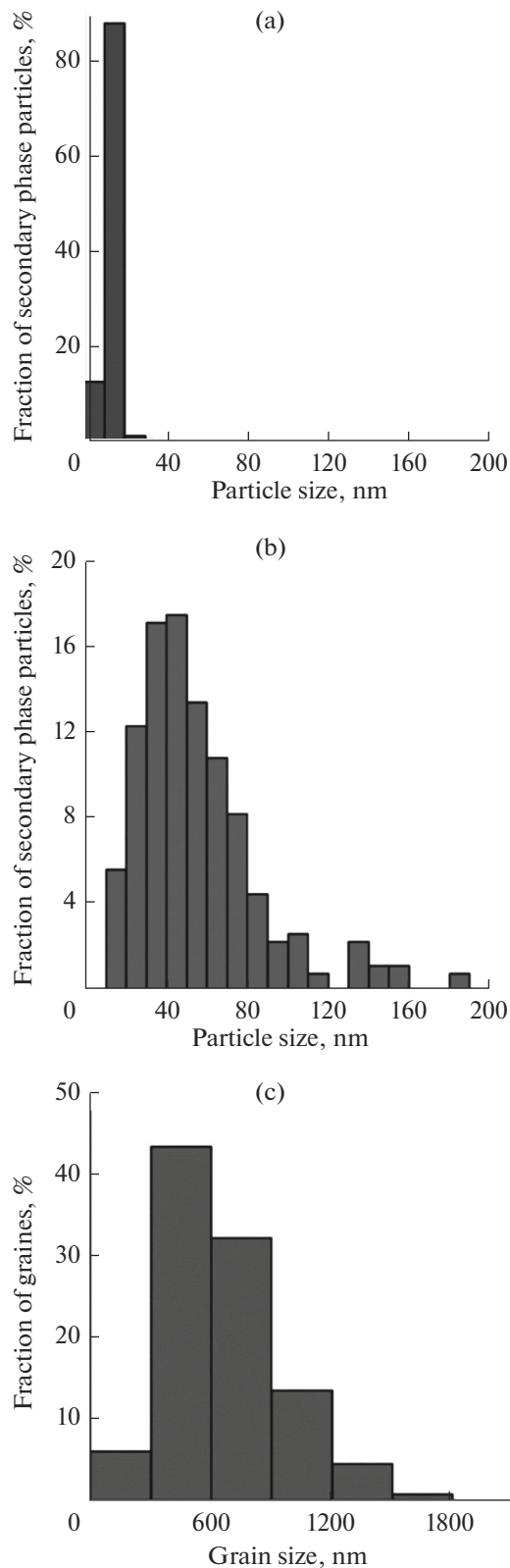


Fig. 3. (a) Al_3Zr particle size distribution histograms for Al–0.4Zr alloys annealed at 648 K for 60 h and (b) grain size and (c) Al_3Zr size distributions after pre-annealing and HPT processing.

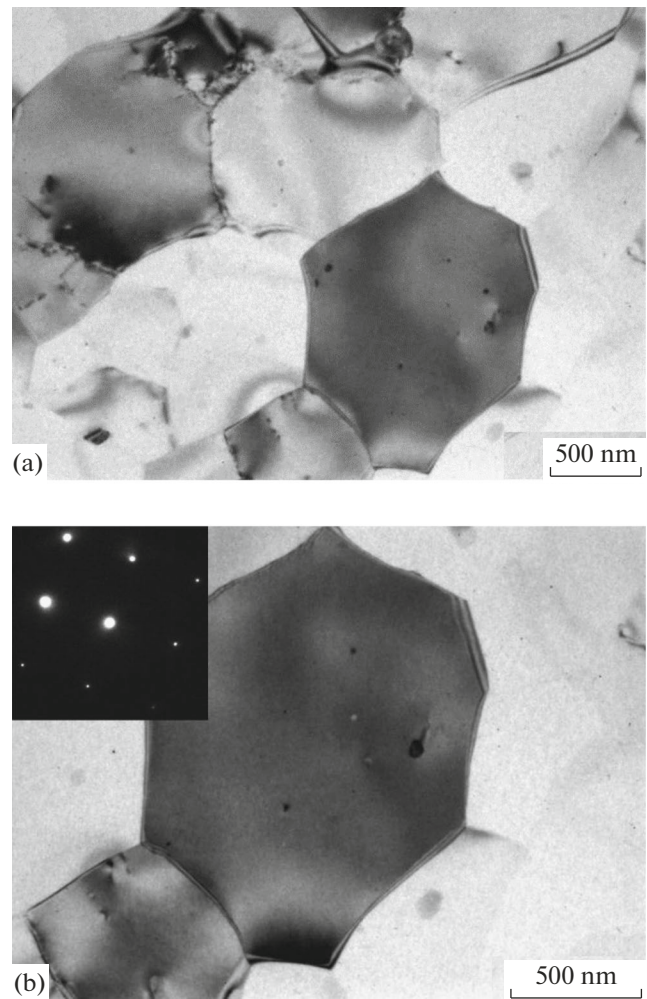


Fig. 4. Microstructure of Al–0.4 wt % Zr alloy after pre-annealing and HPT: (a) light-field image; (b) bright-field image and microdiffraction pattern ([001] zone axis) (TEM).

UFG structure also contains coarse dispersed particles (see Fig. 3) that are likely the particles of redundant crystallite phases refined by HPT. Their dispersion after deformation was also observed in other aluminum alloys [8, 22, 23].

Mechanical Properties

Figure 5 displays the microhardness measured in the initial samples, after 60 h of annealing at 648 K, and after HPT and additional short-term annealing at temperatures of 363–673 K. The pristine Al–0.4Zr samples demonstrate fairly high microhardness ($H_v \approx 469$ MPa), which exceeds to a large extent that of commercially pure Al ($H_v = 205$ MPa) [20]. The pre-annealing at 648 K for 60 h leads to a decrease in microhardness of the initial samples by ~15%, and successive HPT processing augments the microhardness by ~10%, reaching ~439 MPa. The additional

Table 2. Microstructural parameters of Al–0.4Zr alloy

Treatment	Average grain size, nm	Average aluminide size, nm	Average distance between aluminides, nm	Secondary phase particle fraction (by area), %
648 K, 60 h	CG	13 ± 2	38 ± 11	8.74
648 K, 60 h + HPT	663 ± 237	56 ± 23	425 ± 188	0.71

annealing at temperatures of 363–503 K for an hour causes a gain in microhardness, and its maximum of ~508 MPa is achieved after annealing at 423 K. The results of the uniaxial tensile tests are summarized in Fig. 5b and Table 3. The changes in yield stress and ultimate tensile strength are consistent with the change in microhardness. It is worth mentioning a high degree of plasticity in samples after pre-annealing for 60 h at 648 K and HPT ($\delta \approx 28\%$). The additional annealing at 503 K leads to a slight reduction in plasticity (to ~18%), and the ultimate tensile strength and yield stress are found to be ~142 and ~137 MPa, respectively.

According to [24], the annealing at 503 K for an hour corresponds to 400 h of temperature exposure at 453 K. In this respect, one can conclude that the UFG Al–0.4Zr alloy can possess stable mechanical characteristics, while being employed for a long time at a temperature of 423 K. An increase in strength of UFG Al upon an hour of annealing at low temperatures was observed earlier in [19, 21, 25], where the hardening effect by the annealing was explained by the sinking of intragranular mobile dislocations to the neighboring high-angle grain boundaries [25] and/or their dislocation structure reconstruction from a nonequilibrium to an equilibrium one [19, 21]. In the present work, an increase in strength of the UFG Al–0.4Zr alloy can be due to these processes, but one also cannot exclude the formation of grain-boundary segregations, clusters, and/or nanoscale precipitates at the grain boundaries (including the Al_3Zr nanoprecipitates) by Zr atoms that have passed into the aluminum solid solution during HPT. In connection with this, the fine structure study of grain boundaries via analytical electron microscopy will be implemented in our forthcoming works.

Electrical Properties

Figure 6 displays the specific electric resistance at (a) 293 and (b) 77 K after HPT and annealing. The initial Al–0.4Zr samples exhibit a specific resistance 26% greater than that in coarse-grained commercially pure Al [20], which is first of all on account of the presence of Zr atoms in the aluminum solid solution [2–4]. The long-term annealing at 648 K leads to a decrease in specific resistance by ~14% because of

reduced Zr atom concentration in the aluminum matrix owing to the formation of Al_3Zr nanoparticles (Fig. 2). The HPT of annealed samples causes an increase in specific resistance by ~5%, but even in this case, the latter remains at the level lower than in the initial sample (Fig. 6). A gain in specific resistance in UFG alloys seems to be due to increased grain boundary density and partial dissolution of Al_3Zr nanoparticles (Fig. 4). A further annealing at temperatures to 473 K causes no significant change in specific resis-

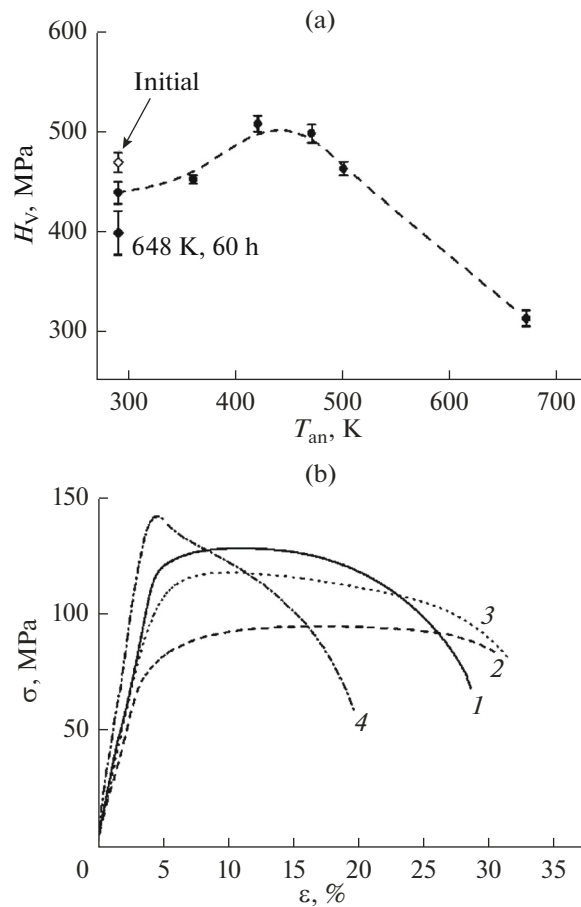


Fig. 5. (a) Microhardness as a function of annealing temperature of HPT-processed Al–0.4Zr samples and (b) stress–strain diagrams of (1) initial sample; (2) sample pre-annealed at 648 K for 60 h and then processed by (3) HPT at 6 GPa and additionally annealed (4) at 503 K.

Table 3. Mechanical and electrical properties of Al–0.4Zr alloy

Treatment	H_V , MPa	$\sigma_{0.2}$, MPa	σ_{UTS} , MPa	δ , %	ρ_{293} , n Ω m	% IACS	ρ_{77} , n Ω m
Initial alloy	469 ± 10	117 ± 2	128 ± 2	26 ± 1	34.03	50.7	9.52
648 K, 60 h	399 ± 22	72 ± 6	95 ± 4	27 ± 2	29.31	58.8	4.26
648 K, 60 h + HPT	439 ± 11	96 ± 2	118 ± 2	28 ± 1	30.93	55.8	6.92
648 K, 60 h + HPT + 423 K, 1 h	508 ± 8	–	–	–	31.02	55.6	7.08
648 K, 60 h + HPT + 503 K, 1 h	463 ± 7	137 ± 2	142 ± 1	18 ± 1	29.60	58.3	5.90

tance, but leads to an increase in microhardness (Fig. 5a). The annealing at 503 K almost recovers the high level of electrical conductivity ($\sim 58.3\%$ IACS) attained in the alloy annealed at 648 K. The specific electrical resistance measured at 77 K exhibits a similar tendency (Fig. 6b, Table 3).

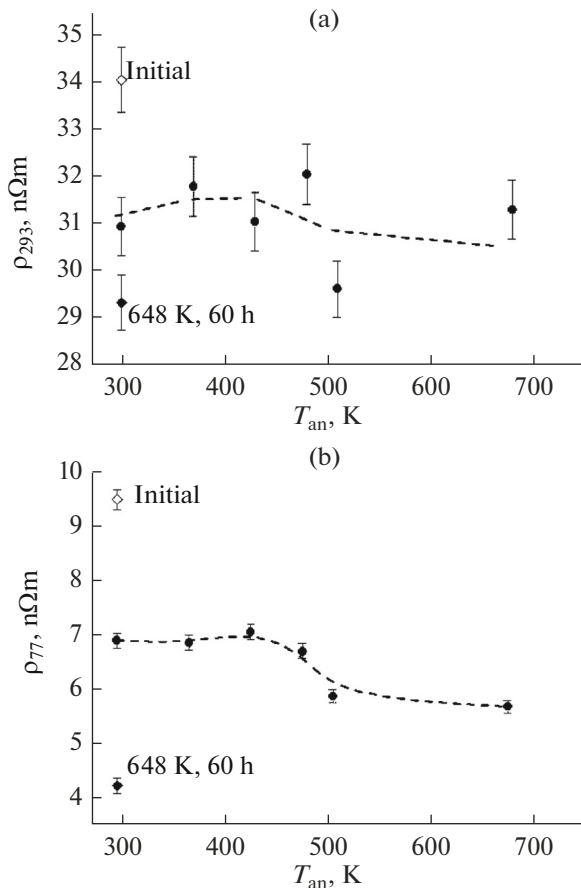


Fig. 6. Electrical resistivity at (a) 293 and (b) 77 K as a function of additional annealing temperature for pre-annealed and HPT-processed Al–0.4Zr alloy.

CONCLUSIONS

The pioneering study of the influence of severe plastic deformation by torsion and subsequent annealing on the mechanical properties and electrical conductivity of the aluminum alloy doped with 0.4 wt Zr was performed. The annealing at 648 K for 60 h was found to cause the formation of Al_3Zr spherical nanoparticles of metastable modification $L1_2$ with the average diameter of ~ 13 nm, as well as to ensure a high electrical conductivity (58.8% IACS).

Besides the formation of a uniform UFG structure with the average grain size of 660 nm, the room-temperature HPT led to partial dissolution of Al_3Zr nanoparticles and, consequently, to a gain in strength (by $\sim 10\%$) and to a decrease in electrical conductivity to 55.8% IACS.

The subsequent annealing for an hour at a temperature of 503 K ensured a further increase in yield strength by 20% and the recovery of electrical conductivity to the value close to that of annealed specimen (58.3% IACS).

The thermal stability of the mechanical properties of the UFG Al–0.4Zr alloy processed by HPT was shown as well, which opens up the prospects for improving the functional properties of conductors based on aluminum–zirconium alloys.

ACKNOWLEDGMENTS

M.Yu. Murashkin and R.Z. Valiev are grateful to the Russian Science Foundation for the financial support of this work (project no. 17-19-01311). Structural characterization via transmission electron microscopy was performed using the facilities at the Center for Shared Use Nanotech at Ufa State Aviation Technical University (<http://nanotech.ugatu.ac.ru>).

REFERENCES

1. Kiessling, F., Nefzger, P., Nolasco, J.F., and Kaintzyk, U., *Overhead Power Lines: Planning, Design, Construction*, Berlin: Springer-Verlag, 2003.

2. Belov, N.A., Alabin, A.N., Eskin, D.G., and Istomin-Kastrovskii, V.V., Optimization of hardening of Al–Zr–Sc cast alloys, *J. Mat. Sci.*, 2006, vol. 41, pp. 5890–5899.
3. Belov, N.A., Alabin, A.N., and Teleuova, A.R., Comparative analysis of alloying additives as applied to the production of heat-resistant aluminum-base wires, *Met. Sci. Heat Treat.*, 2012, vol. 53, nos. 9–10, pp. 455–459.
4. Knych, T., Piwowarska, M., and Uliasz, P., Studies on the process of heat treatment of conductive AlZr alloys obtained in various productive processes, *Arch. Metall. Mater.*, 2011, vol. 56, pp. 685–692.
5. Zhou, W.W., Cai, B., Li, W.J., Liu, Z.X., and Yang, S., Heat-resistant Al–0.2Sc–0.04Zr electrical conductor, *Mat. Sci. Eng., A*, 2012, vol. 552, pp. 353–358.
6. Ryabov, D.K., Antipov, K.V., Fesenko, T.V., and Dynin, N.V., Influence of cobalt alloying on structure and long-term strength of Al–Cu–Mg–Ag alloy system, *Inorg. Mater.: Appl. Res.*, 2017, vol. 8, no. 1, pp. 159–165.
7. Kaygorodova, L.I., Pilyugin, V.P., Pushin, V.G., and Rasposienko, D.Yu., Stability of nanocrystalline structure and phase transformations in high-strength alloy Al–Li–Cu–Zr, *Inorg. Mater.: Appl. Res.*, 2014, vol. 5, no. 1, pp. 28–31.
8. Murashkin, M.Y., Sabirov, I., Medvedev, A.E., Enikeev, N.A., Lefebvre, W., Valiev, R.Z., and Sauvage, X., Mechanical and electrical properties of an ultrafine grained Al–8.5 wt % RE (RE = 5.4 wt % Ce, 3.1 wt % La) alloy processed by severe plastic deformation, *Mater. Des.*, 2016, vol. 90, pp. 433–442.
9. Knipling, K.E., Dunand, D.C., and Seidman, D.N., Precipitation evolution in Al–Zr and Al–Zr–Ti alloys during isothermal aging at 375–425°C, *Acta Mater.*, 2008, vol. 56, pp. 114–127.
10. Tecer, H., Acer, E., Erol, H., and Gündüz, M., Effect of aging on conductivity of heat resistant overhead line conductors, *Mater. Sci. Forum*, 2013, vol. 765, pp. 783–787.
11. Valiev, R.Z., Islamgaliev, R.K., and Alexandrov, I.V., Bulk nanostructured materials from severe plastic deformation, *Prog. Mat. Sci.*, 2000, vol. 45, pp. 103–189.
12. Murashkin, M.Yu., Sabirov, I., Sauvage, X., and Valiev, R.Z., Nanostructured Al and Cu alloys with superior strength and electrical conductivity, *J. Mater. Sci.*, 2016, vol. 51, pp. 33–49.
13. Murashkin, M.Yu., Medvedev, A.E., Kazykhanov, V.U., Raab, G.I., Ovid'ko, I.A., and Valiev, R.Z., Microstructure, strength, electrical conductivity and heat resistance of an Al–Mg–Zr alloy after ECAP-conform and cold drawing, *Rev. Adv. Mater. Sci.*, 2016, vol. 47, pp. 16–25.
14. Brodova, I.G., Shirinkina, I.G., and Antonova, O.V., Phase and structural transformations in the Al–Cr–Zr alloy after rapid melt quenching and high-pressure torsion, *Phys. Met. Metallogr.*, 2007, vol. 104, no. 3, pp. 281–288.
15. Brodova, I.G., Stolyarov, V.V., Manukhin, A.B., Yablonskikh, T.I., Bashlykov, D.V., Soshnikova, E.P., and Zolotova, N.A., Formation of ultrafine structure in a rapidly solidified Al–Zr alloy under the effect of severe plastic deformation, *Phys. Met. Metallogr.*, 2001, vol. 91, no. 5, pp. 494–499.
16. Knipling, K.E., Dunand, D.C., and Seidman, D.N., Criteria for developing castable, creep-resistant aluminum-based alloys—a review, *Int. J. Mater. Res.*, 2006, vol. 97, pp. 246–265.
17. Brown, L.M., Ham, R.K., Kelly, A., and Nicholson, R.B., *Strengthening Methods in Crystals*, New York: Elsevier, 1971, pp. 9–133.
18. Zhilyaev, A.P. and Langdon, T.G., Using high-pressure torsion for metal processing: Fundamentals and applications, *Prog. Mater. Sci.*, 2008, vol. 53, pp. 893–979.
19. Mavlyutov, A.M., Latynina, T.A., Murashkin, M.Yu., Orlova, T.S., and Valiev, R.Z., Effect of annealing on the microstructure and mechanical properties of ultrafine-grained commercially pure Al, *Phys. Solid State*, 2017, vol. 59, no. 10, pp. 1970–1977.
20. Orlova, T.S., Mavlyutov, A.M., Bondarenko, A.S., Kasatkin, I.A., Murashkin, M.Yu., and Valiev, R.Z., Influence of grain boundary state on electrical resistivity of ultrafine grained aluminium, *Philos. Mag.*, 2016, vol. 96, pp. 2429–2444.
21. Mavlyutov, A.M., Bondarenko, A.S., Murashkin, M.Yu., Boltynjuk, E.V., Valiev, R.Z., and Orlova, T.S., Effect of annealing on microhardness and electrical resistivity of nanostructured SPD aluminum, *J. Alloys Compd.*, 2017, vol. 698, pp. 539–546.
22. Zhilyaev, A.P., García-Infanta, J.M., Carreño, F., Langdon, T.G., and Ruano, O.A., Particle and grain growth in an Al–Si alloy during high-pressure torsion, *Scr. Mater.*, 2007, vol. 57, pp. 763–765.
23. Cepeda-Jiménez, C.M., García-Infanta, J.M., Zhilyaeva, A.P., Ruano, O.A., and Carreño, F., Influence of the supersaturated silicon solid solution concentration on the effectiveness of severe plastic deformation processing in Al–7 wt % Si casting alloy, *Mat. Sci. Eng., A*, 2011, vol. 528, pp. 7938–7947.
24. *IEC 62004: Thermal-Resistant Aluminum Alloy Wire for Overhead Line Conductor*, Geneva: Int. Electrotech. Comm., 2007.
25. Huang, X., Hansen, N., and Tsuji, N., Hardening by annealing and softening by deformation in nanostructured metals, *Science*, 2006, vol. 312, pp. 249–251.

Translated by O. Maslova